CONDENSED MATTER PHYSICS

Spin excitation continuum from degenerate states in the mixed ferro-antiferromagnetic exchange system $CeMgAl_{11}O_{19}$

Bin Gao[1,2]†, Tong Chen[1,2,3]†, Chunxiao Liu[4]†‡, Mason L. Klemm[1,2], Shu Zhang[5], Zhen Ma[6]*, Xianghan Xu[7,8]§, Choongjae Won[9], Gregory T. McCandless[10], Karthik Rao[1,2], Naoki Murai[11], Seiko Ohira-Kawamura[11], Stephen J. Moxim[12], Jason T. Ryan[12], Xiaozhou Huang[13], Xiaoping Wang[14], Manh Duc Le[15], Emilia Morosan[1,2], Julia Y. Chan[10], Sang-Wook Cheong[7], Oleg Tchernyshyov[3], Leon Balents[16,17,18]*, Pengcheng Dai[1,2]*

In the search for unconventional magnetism, exotic quantum states are characterized by a lack of order and a broad spin excitation continuum approaching zero temperature. We study the two-dimensional triangular-lattice effective spin-$\frac{1}{2}$ system $CeMgAl_{11}O_{19}$, which shows slight disorder but no magnetic ordering down to 100 millikelvin. Spin-wave analysis in the magnetic-field–polarized state determines the spin Hamiltonian featuring a mixed ferromagnetic-antiferromagnetic nearest-neighbor exchange interaction [$J_z = -0.024(5)$ milli–electron volts, $J_\perp = 0.056(3)$ milli–electron volts]. This places the system near an exactly solvable point of the spin-$\frac{1}{2}$ triangular-lattice *XXZ* model ($J_z = -\frac{1}{2}J_\perp$) with extensive ground-state degeneracy. In zero field, neutron spectroscopy reveals a prominent continuum; we show that this arises from an ensemble average of spin-wave spectra across the degenerate ground-state manifold. This demonstrates that the role of weak quenched disorder can be quantitatively constrained: It inhibits unique ground-state selection and stabilizes a local distribution within the degenerate manifold, yielding continuum-like spectra that necessitate a critical reevaluation of the experimental signatures of exotic quantum states.

INTRODUCTION

Quantum magnets host a variety of unconventional phases: quantum spin liquids (QSLs) (*1*–*2*), quadrupolar orders (*3*–*5*), and spin glasses (*6*–*7*), to name a few, all of which expand our understanding of quantum phases of matter. QSLs, in particular, feature emergent gauge fields and fractionalized spin-1/2 excitations, and they have often come to stand in for "the" exotic state (*8*–*12*). The experimental search for QSLs is a major effort given their promising applications to fault-tolerant quantum computation (*13*), yet a definitive identification remains challenging: The widely cited hallmark of a broad, featureless continuum of spin excitations in inelastic neutron scattering is not unique to fractionalization; magnetic and structural disorder can generate similar spectra, inviting interpretations beyond QSLs (*14*–*24*).

In this work, we report a material-specific alternative to the fractionalization interpretation. We study the Ce-based effective spin-1/2 triangular-lattice hexaaluminate $CeMgAl_{11}O_{19}$ (Fig. 1A) (*25*–*31*) and show that weak quenched disorder frustrates unique ground-state selection, stabilizing a quasidegenerate liquid without magnetic order. We find that locally selected umbrella configurations persist and that the inelastic neutron response is an ensemble average of conventional spin-wave spectra (Fig. 1B). This mechanism produces a QSL-like continuum without invoking spinon fractionalization, and we demonstrate that it yields qualitative signatures, distinguishing it from a genuine QSL.

We substantiate this picture with thermodynamic probes and inelastic neutron scattering, which show no magnetic order down to 100 mK and reveal a spin excitation continuum gapped throughout the Brillouin zone except at Γ features that, taken alone, could appear QSL like (*8*–*12*). We then establish that $CeMgAl_{11}O_{19}$ is captured by a spin-1/2 triangular-lattice *XXZ* model with mixed ferromagnetic (FM)–antiferromagnetic (AFM) exchange (Fig. 1A)

$$\mathcal{H} = \sum_{<i,j>} \left[J_z S_i^z S_j^z + J_\perp \left(S_i^x S_j^x + S_i^y S_j^y \right) \right] \quad (1)$$

where the sum is over adjacent sites, S_i^α is a spin-*S* operator, and J_z ($J_\perp$) denotes out-of-plane (in-plane) exchange interactions. Figure 1B shows the phase diagram for the spin-1/2 *XXZ* model on a two-dimensional (2D) triangular lattice, where the exchange interactions

[1]Department of Physics and Astronomy, Rice University, Houston, TX, USA. [2]Rice Laboratory for Emergent Magnetic Materials and Smalley-Curl Institute, Rice University, Houston, TX, USA. [3]Institute for Quantum Matter and Department of Physics and Astronomy, Johns Hopkins University, Baltimore, MD, USA. [4]Department of Physics, University of California, Berkeley, Berkeley, CA, USA. [5]Collective Dynamics and Quantum Transport Unit, Okinawa Institute of Science and Technology Graduate University, Onna-son, Okinawa, Japan. [6]Hubei Key Laboratory of Photoelectric Materials and Devices, School of Materials Science and Engineering, Hubei Normal University, Huangshi, China. [7]Keck Center for Quantum Magnetism and Department of Physics & Astronomy, Rutgers University, Piscataway, NJ, USA. [8]Department of Chemistry, Princeton University, Princeton, NJ, USA. [9]Laboratory for Pohang Emergent Materials and Max Planck POSTECH Center for Complex Phase Materials, Pohang University of Science and Technology, Pohang, Korea. [10]Department of Chemistry and Biochemistry, Baylor University, Waco, TX, USA. [11]J-PARC Center, Japan Atomic Energy Agency, Tokai, Ibaraki, Japan. [12]Alternative Computing Group, National Institute of Standards of Technology, Gaithersburg, MD, USA. [13]Chemical Sciences and Engineering Division, Argonne National Laboratory, Lemont, IL, USA. [14]Neutron Scattering Division, Oak Ridge National Laboratory, Oak Ridge, TN, USA. [15]ISIS Neutron and Muon Source, Didcot, Oxfordshire OX11 0QX, UK. [16]Kavli Institute for Theoretical Physics, University of California, Santa Barbara, Santa Barbara, CA, USA. [17]Canadian Institute for Advanced Research, Toronto, Ontario, Canada. [18]French American Center for Theoretical Science, CNRS, KITP, Santa Barbara, CA, USA.
*Corresponding author. Email: zma@hbnu.edu.cn (Z.M.); balents@spinsandelectrons.com (L.B.); pdai@rice.edu (P.D.)
†These authors contributed equally to this work.
‡Present address: Université Paris-Saclay, CNRS, Laboratoire de Physique des Solides, 91405 Orsay, France.
§Present address: School of Physics and Astronomy, University of Minnesota, Minneapolis, MN, USA.

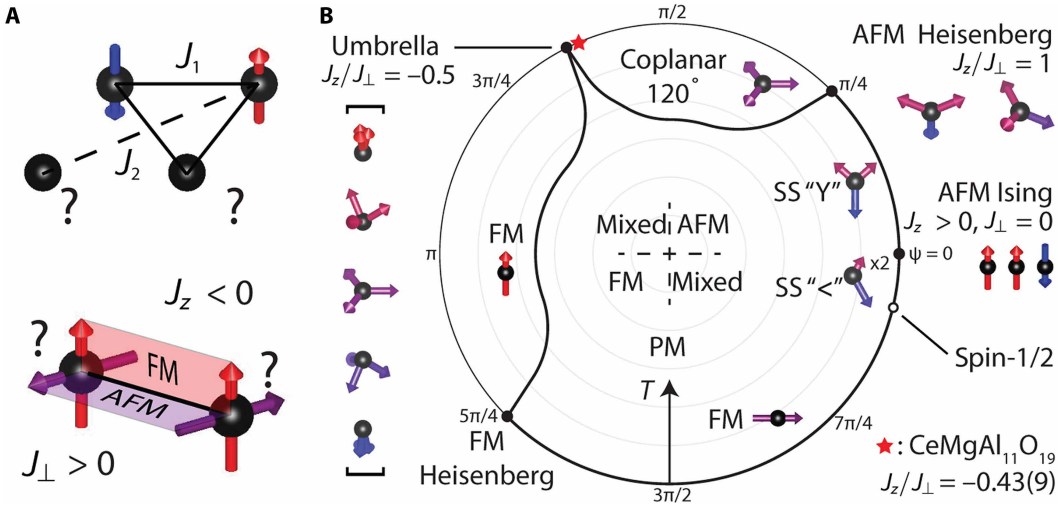

Fig. 1. Frustration mechanisms and the phase diagram of *XXZ* model on a triangular lattice. (**A**) Schematic illustrating sources of frustrations, including lattice geometry, competing interactions (top), and the mixed FM-AFM exchange (bottom). (**B**) Phase diagram of the spin-$\frac{1}{2}$ *XXZ* model on a triangular lattice, reproduced from (*40*, *44*, *45*). The exchange interactions are parameterized as $J_z = \cos\psi$ and $J_\perp = \sin\psi$. The diagram includes FM, paramagnetic (PM), and supersolid (SS) phases. The thick solid line indicating transition temperatures is decorated with phase boundaries including three disordered states at $\psi = 0, \frac{1}{4}\pi$, and ψ_U. The phase boundary between the coplanar FM and SS "<" phases (open circle) is different for spin-$\frac{1}{2}$ and classical spins ($S \to \infty$), and the ground state on the boundary remains elusive. The position of $CeMgAl_{11}O_{19}$ in this phase diagram is marked by the red star.

are parameterized as $J_z = \cos\psi$ and $J_\perp = \sin\psi$. We find that the spin excitation continuum in $CeMgAl_{11}O_{19}$ arises from an ensemble average of distinct spin-wave spectra corresponding to the degenerate states at a nearby exactly solvable point (ψ_U, i.e., $J_z = -0.5J_\perp, J_\perp > 0$) in the phase diagram, providing a rare example in frustrated magnets where the origin of the spin excitation continuum can be identified.

RESULTS

We successfully synthesized high-quality single crystals of $CeMgAl_{11}O_{19}$, a member of the rare-earth triangular-lattice hexaaluminate family $REMg(Zn)Al_{11}O_{19}$ (RE = Ce, Pr, and Nd) (*25*–*31*). Previous studies on $PrMg(Zn)Al_{11}O_{19}$ (*26*, *28*–*30*) suggest that it may host a QSL state but with the presence of quenched disorder, including ~7% Pr vacancy in the triangular-lattice planes and site mixing between nonmagnetic Mg^{2+} and Al^{3+} ions (*25*, *26*, *28*). While $CeMgAl_{11}O_{19}$ features a more robust Kramers doublet ground state protected by time-reversal symmetry, neutron and x-ray diffraction reveal a similar level of disorder: ~7% Ce vacancy and Mg^{2+} and Al^{3+} site mixing (see Materials and Methods). In a comparable system $YbMgGaO_4$, site mixing of Mg^{2+} and Ga^{3+} ions displaces surrounding oxygen anions within the Yb-O-Yb superexchange paths (*32*). This leads to a distribution of exchange interaction *J*, which induces a spin glass state hinted by the frequency-dependent alternating-current (ac) susceptibility measurements (*19*) and produces continuum-like spin excitations in the inelastic neutron spectrum (*17*–*21*). In contrast, the site mixing in $CeMgAl_{11}O_{19}$ is confined to the Al/MgO_4 tetrahedra and is screened by disorder-free planes of AlO_5 and AlO_6 polyhedra (Fig. 2A), which should have a minimal effect on the magnetic exchange.

We investigated the magnetic and thermodynamic properties of $CeMgAl_{11}O_{19}$ (see Materials and Methods). Figure 2 (B and C) shows the direct-current (dc) magnetic susceptibility $\chi(T)$ and its inverse $1/\chi(T)$, respectively. A fit of the high-temperature data to the Curie-Weiss law yields $\Theta_{CW,\parallel} = 45(1)$ K with an effective moment $\mu_{eff,\parallel} = 2.38(1)\,\mu_B$ for fields parallel to the *c* axis and $\Theta_{CW,\perp} = -110(3)$ K with $\mu_{eff,\perp} = 1.90(2)\,\mu_B$ for fields perpendicular to the *c* axis. χ is significantly larger for a *c* axis–oriented field, suggesting a local easy *c* axis anisotropy. This is also apparent in magnetization $M(B)$ shown in Fig. 2D, which saturates below 4 T at 2 K for a field along the *c* axis but remains unsaturated up to 8 T for an in-plane field. Dashed lines in Fig. 2 (B and D) show a simultaneous fit of $\chi(T)$ and $M(B)$ to a crystal electric field (CEF) model. However, the CEF parameters could not be uniquely determined, and direct measurement of the CEF scheme using thermal neutron scattering spectroscopy is also challenging (see fig. S6 for CEF analysis details) (*31*). To test for a spin glass phase, we measured the ac susceptibility. As shown in Fig. 2E, the absence of a frequency-dependent peak in the real part χ' indicates no spin freezing down to 0.4 K.

The specific heat capacity $C_p(T)$ in zero field, shown in Fig. 2F, displays a broad peak near 0.2 K. This feature is characteristic of the magnetic entropy release and suggests the onset of coherent quantum fluctuations without a magnetic phase transition down to 0.06 K. This peak shifts to higher temperatures with an increasing magnetic field along the *c* axis. The integrated magnetic entropy $S(T)$, shown in Fig. 2G, recovers ~90% of $R\ln 2$ by 10 K, consistent with the Ce^{3+} valence state. The absence of a low-temperature Schottky tail or any excess entropy confirms the magnetic origin of the broad peak in $C_p(T)$.

We explored low-temperature magnetic excitations in zero field using inelastic neutron scattering (see Materials and Methods). Figure 3 (A to F) presents the magnetic scattering in the (*hk*) plane at 0.1 K. Consistent with $C_p(T)$, no magnetic Bragg peaks are observed at the candidate ordering wave vectors in zero field down to 0.10 K, giving an upper bound of 0.01 μ_B per Ce on any static ordered moment within the resolution of our instrument (Fig. 3A). As energy increases from 0.03 to 0.09 meV, a sharp, spin-wave–like mode forms rings of scattering stemming from the Γ points (Fig. 3, B to E).

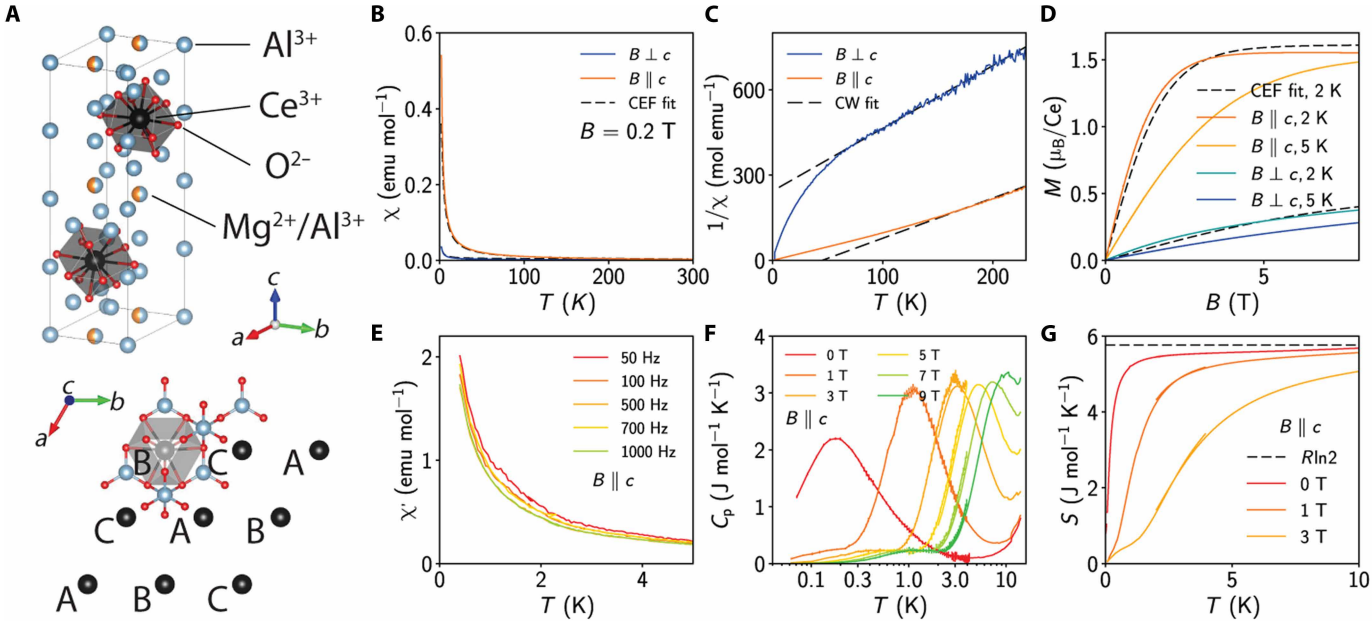

Fig. 2. Crystal structure and thermodynamic properties of $CeMgAl_{11}O_{19}$. (**A**) Crystal structure showing Ce^{3+} ions forming triangular-lattice planes, with CeO_{12} polyhedra highlighted. (**B**) Temperature dependence of magnetic susceptibility $\chi(T)$ measured in a 0.2-T field applied parallel and perpendicular to the *c* axis. The SI equivalent of electromagnetic units per mole is 4π cm^3 mol^{-1}. (**C**) Inverse susceptibility $1/\chi(T)$, with solid lines representing Curie-Weiss fits to the high-temperature data. (**D**) Field-dependent magnetization $M(B)$ at 2 and 5 K. Saturating below 4 T for the field along the *c* axis indicates an easy-axis anisotropy. (**E**) Real part of the ac susceptibility $\chi'(T)$ at various frequencies, showing no evidence of spin freezing. (**F**) Specific heat capacity $C_p(T)$ in various magnetic fields applied along the *c* axis. The data show a broad peak characteristic of magnetic contributions. (**G**) Magnetic entropy $S(T)$ obtained by integrating the heat capacity data.

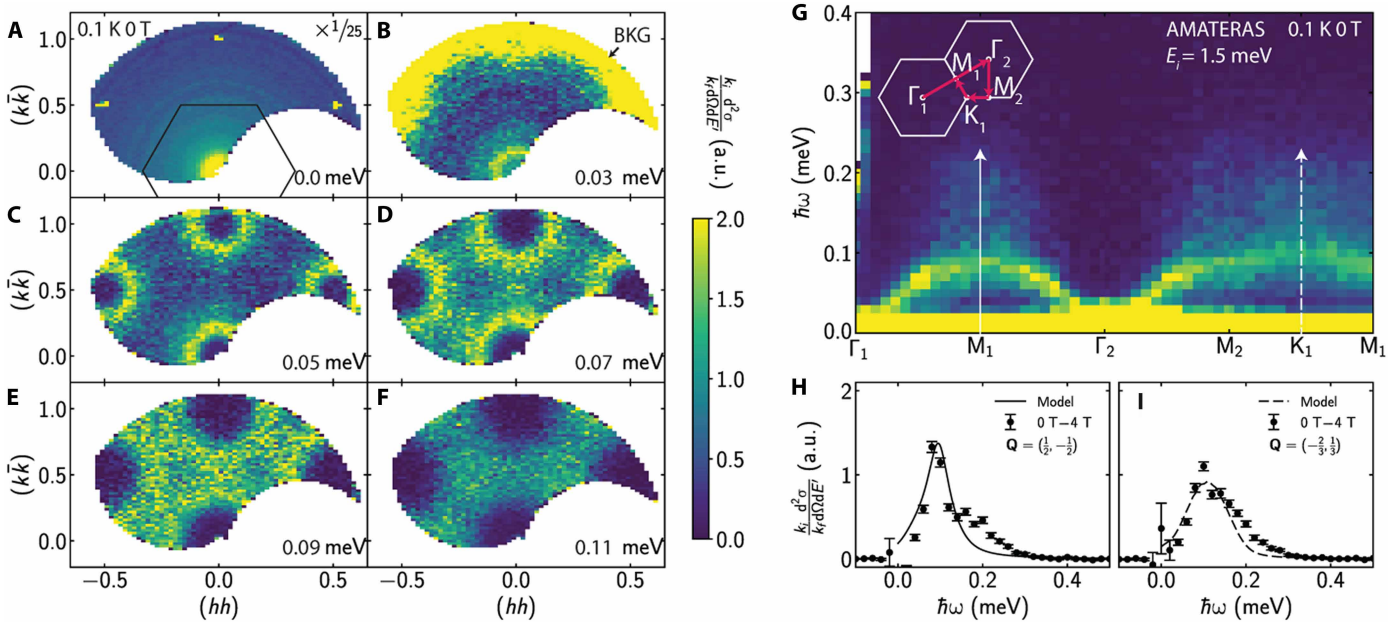

Fig. 3. Magnetic excitations of $CeMgAl_{11}O_{19}$ as a function of energy (*E*) and momentum (Q) in zero field. (**A** to **F**) Constant-*E* slices in the (*hk*) plane at 0.1 K, showing the evolution of the magnetic scattering. a.u., arbitrary units. (**G**) *E*-**Q** spectrum along high-symmetry directions in the Brillouin zone. (**H** and **I**) Constant-**Q** cuts at the M_1 and K_1 points, respectively. The solid and dashed lines are corresponding cuts from the calculated spectrum shown in Fig. 5A.

This is also evident in the *E*-**Q** spectrum along high-symmetry directions ($\Gamma_1 \rightarrow M_1 \rightarrow \Gamma_2 \rightarrow M_2 \rightarrow K_1 \rightarrow M_1$), shown in Fig. 3G. For energies $E = \hbar\omega < 0.1$ meV, the constant-energy slices also reveal spectral weight distributed smoothly across a wide range of momentum, bounded by the sharp mode near the Γ points (Fig. 3, C and D). For $\hbar\omega > 0.1$ meV, broad and featureless excitations persist around the zone boundaries up to 0.3 meV (Fig. 3, F to I). This spectrum is reminiscent of the spin excitation continua observed in other 2D QSL candidates, such as $ZnCu_3(OH)_6Cl_2$ (*14*), $YbMgGaO_4$ (*17*, *18*), and $NaYbSe_2$ (*33*), where such features have been interpreted as the hallmark of fractionalized excitations.

Notably, the continuum-like excitations in $CeMgAl_{11}O_{19}$ appear to be gapped at the M and K points (Fig. 3, H and I). While most QSL candidates exhibit predominantly quasielastic scattering, which concentrates at $\hbar\omega = 0$ meV at the zone boundaries (*14*, *17*, *18*, *33*), advanced numerical studies for QSLs on a triangular lattice predict broad peaks at finite *E* at both M and K (*34*, *35*). On the basis of the absence of magnetic ordering or spin freezing, combined with the similarity between the observed spectrum and theoretical predictions, one would reasonably classify $CeMgAl_{11}O_{19}$ as a strong QSL candidate. The remainder of this work is dedicated to demonstrating why this conventional conclusion would be incorrect by providing a more careful examination of the spin excitation continuum and the role of disorder.

To rigorously test the QSL hypothesis, we first determined the spin Hamiltonian by measuring spin-wave excitations in the magnetic-field–polarized FM state. Figure 4A shows the spectrum at 0.1 K in a 4-T field, which is sufficient to polarize the system. The spectrum exhibits a sharp, well-defined spin-wave mode as expected for a field-polarized state. While the dispersion has minimal energy at the zone boundaries and peaks at the Γ point, consistent with an AFM exchange *J*, the **Q**-averaged energy is higher than the Zeeman energy of $2g_z S\mu_B B = 0.847$ meV [calculated with $g_z = 3.66$, determined by electron spin resonance (see fig. S4 for details)]. This indicates that flipping a spin costs additional energy, which is indicative of an FM exchange. This apparent contradiction suggests that the minimal description is the *XXZ* model (Eq. 1) with a mixed FM-AFM exchange ($\frac{1}{2}\pi < \psi < \pi$).

Furthermore, the spin-wave excitations are resolution limited, differentiating $CeMgAl_{11}O_{19}$ from other QSL candidates where disorder broadens the modes (*18*, *36*, *37*). The sharp spin wave indicates a negligible effect of disorder on the exchange interactions and permits a precise determination of the spin Hamiltonian. We performed a pixel-to-pixel least squares fit of the data in Fig. 4A to linear spin-wave theory (*38*), convoluting the calculated cross section with a Gaussian function with the instrumental energy resolution (0.07-meV full width at half maximum). This procedure yields an excellent account of the data, as shown in Fig. 4B, with exchange parameters $J_z = -0.02$ (5) meV and $J_\perp = 0.056(3)$ meV. Including the symmetry-allowed nearest-neighbor terms $J_{\pm\pm}$ and no D_z, we obtain $J_{\pm\pm} = 0.006(2)$ meV, confirming *XXZ* dominance (full symmetry-allowed fit and inversion formulas are given in the Supplementary Materials). The resulting exchange anisotropy $J_z/J_\perp = -0.43(4)$ places $CeMgAl_{11}O_{19}$ very close to the boundary ψ_U between the 120° coplanar order and the out-of-plane FM ordered phases (Fig. 1B).

In 1986, Miyashita (*39*) showed that for the classical *XXZ* model ($S \rightarrow \infty$) on a triangular lattice, the FM and coplanar 120° states are both frustrated at ψ_U ($J_z = -0.5J_\perp$ and $J_\perp > 0$), where the system

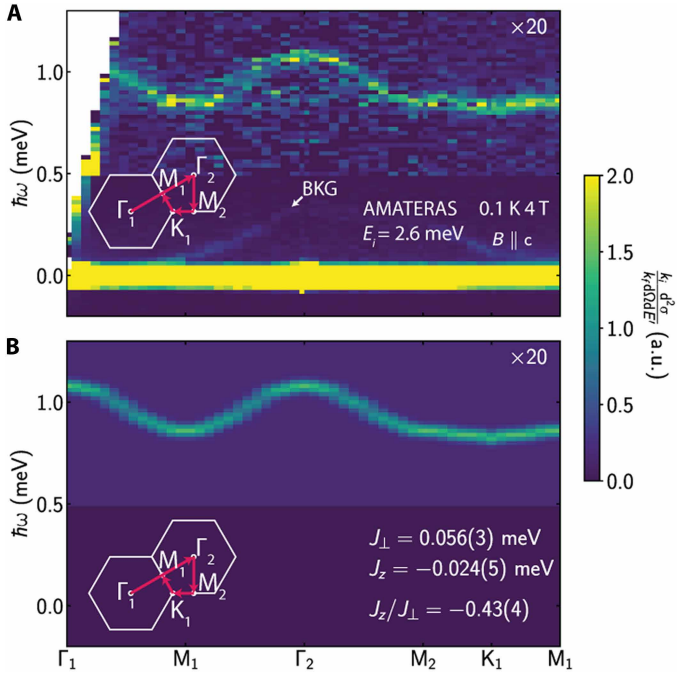

Fig. 4. Coherent spin waves in the field-polarized FM state of $CeMgAl_{11}O_{19}$. (**A**) *E*-**Q** spectrum measured at 0.1 K in a 4-T field applied along the *c* axis. The data reveal sharp, resolution-limited modes, indicating that disorder has a negligible effect on the exchange interactions. The inset shows the measurement path in reciprocal space. A dispersive feature at low energies that does not follow the lattice symmetry is from the sample environment, labeled as "BKG." (**B**) Spin-wave excitations simulated by linear spin-wave theory using spinW library (*38*) with the best-fit parameters $J_z = -0.024(5)$ meV and $J_\perp = 0.056(3)$ meV, obtained from a pixel-to-pixel fit to the experimental data in (A).

exhibits a three-sublattice "umbrella" order. The quantum spin-1/2 case was later shown to be exactly solvable at this point with a ground-state manifold that has the same degeneracy as the classical model by Momoi and Suzuki (*40*). Crucially, thermal fluctuations among these degenerate umbrella states prevent the development of long-range order at finite temperatures, resulting in a quantum disordered state (*41*–*48*).

With the minimal model established, we can now determine the origin of the zero-field spin excitation spectrum. The absence of magnetic ordering and the system's proximity to the highly degenerate point imply that at low temperatures, the system does not settle into a single state but instead samples a vast landscape of isoenergetic configurations. We calculated the ensemble-averaged spectrum for the degenerate manifold at the exactly solvable point ($J_z = -\frac{1}{2}J_\perp$) using the Sunny Suite (*49*). As shown in Fig. 5 (A and B), this calculation quantitatively reproduces the measured spectrum and constant-energy cuts. The calculation assumes a Gaussian distribution of the umbrella states' out-of-plane angle θ (centered at θ = 90° with a 20° SD). While the most intense spin-wave mode persists at the same energy and momentum along the Γ-M direction for all states in the manifold, their dispersion varies markedly along the M-K zone boundary (Fig. 5, C to E). The ensemble average of these distinct spectra naturally results in the observed continuum-like excitations bounded by the sharp mode.

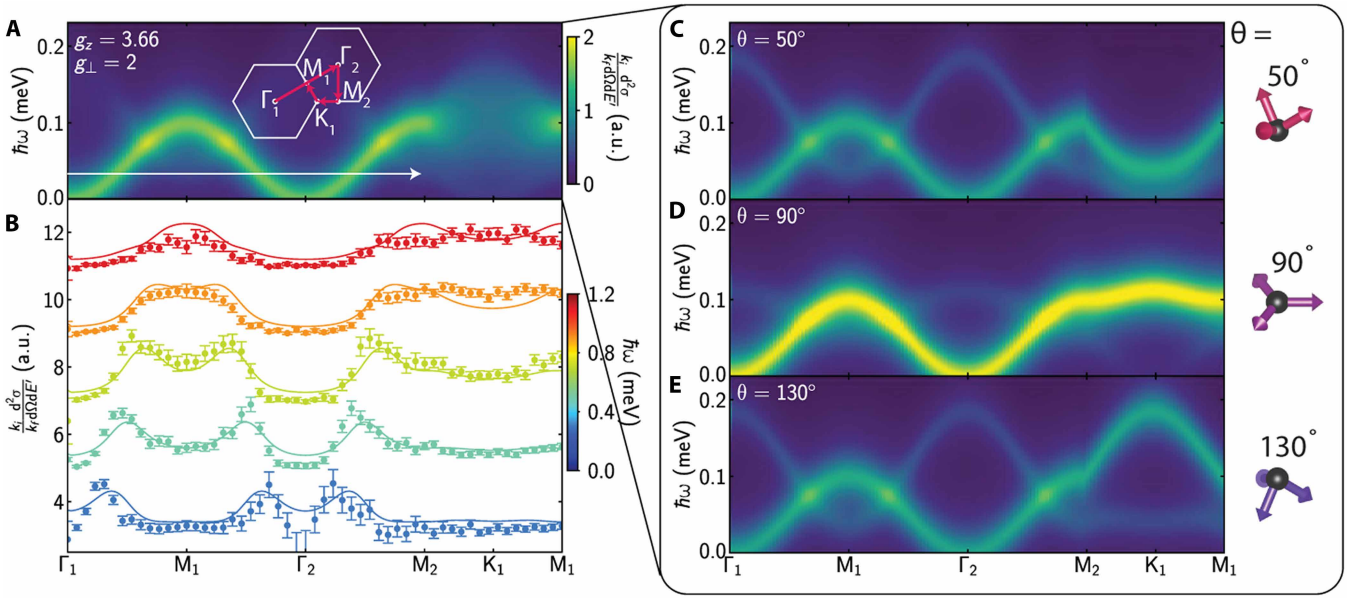

Fig. 5. Calculated ensemble-averaged magnetic excitations of the degenerate ground state. (**A**) Calculated *E*-**Q** spectrum at $\psi = \psi_U$, obtained by averaging the spin-wave spectra of states within the umbrella manifold. The calculation assumes a Gaussian distribution of the spin canting angle θ (centered at 90° with a 20° SD) to describe the experimental data in Fig. 3. (**B**) Comparison of constant-*E* cuts from the experimental data and the ensemble-averaged calculation at various energies. (**C** to **E**) Representative individual spin-wave spectra for specific θ within the degenerate manifold, calculated using the Sunny Suite (*49*). The averaging of such distinct spectra produces the continuum shown in (A).

DISCUSSION

We have shown that while the continuum-like excitations in $CeMgAl_{11}O_{19}$ are qualitatively indistinguishable from the canonical signatures of a QSL, the spectrum is in fact an ensemble average. This finding serves as a critical and necessary cautionary example for the field. It provides a direct experimental demonstration that a spin excitation continuum is an ambiguous signature that can arise from averaging over a degenerate manifold of nearly classical states; see also (*50*–*52*). Therefore, the observation of a continuum and the lack of magnetic ordering are insufficient proof for the existence of a QSL.

Having established that site mixing is modest and that high-field magnons are resolution limited, we conclude that disorder from site mixing does not produce the continuum from an otherwise well-ordered ground state. This is different from 2D triangular-lattice $YbMgGaO_4$ and $YbZnGaO_4$ QSL candidates, where disorder from site mixing between nonmagnetic Mg^{2+} (Zn^{2+}) and Ga^{3+} ions induces considerable broadening of the partially field-polarized spin excitations (*36*, *53*). Strictly speaking, the exactly solvable point of the *XXZ* model at $J_z = -\frac{1}{2}J_\perp$ is slightly different from the observed $J_z/J_\perp = -0.43(4)$ for $CeMgAl_{11}O_{19}$, and it remains to examine the effect of other symmetry-allowed exchange interactions beyond the toy model (*1*). Although a weak quenched disorder in $CeMgAl_{11}O_{19}$ does not broaden the field-induced magnons (Fig. 4), it can prevent unique selection among nearly isoenergetic umbrella states at low temperature, gently biasing the local manifold weights. The resulting spatial/temporal ensemble average of conventional spin-wave responses yields the observed continuum without requiring fractionalized excitations. In an ideal spin system with degenerate ground states, one would expect some infinitesimal perturbations or quantum fluctuations to lift this degeneracy via the "order-by-disorder" mechanism, selecting a single ordered state at the lowest temperatures (*54*–*56*). In such a scenario, any QSL-like behavior and its associated continuum signature would likely exist only in a narrow temperature window, if at all. The presence of a weak, quenched disorder, however, can compete with and frustrate such ordering tendencies. By preventing the system from selecting a single ordered state, the disorder effectively stabilizes the manifold of isoenergetic configurations down to the lowest temperatures, thereby preserving the necessary conditions for the observed phenomena.

In conclusion, our work provides a definitive experimental demonstration that a signature widely considered a hallmark of QSLs—a broad continuum of excitations—can arise from an alternative origin. By identifying $CeMgAl_{11}O_{19}$ as a rare realization of a mixed FM-AFM exchange system, and by showing that its spectrum is a predictable consequence of a nearby degenerate ground-state manifold, the work sheds light on a long-standing ambiguity in the identification of QSLs and underscores the subtle yet crucial role of disorder.

MATERIALS AND METHODS

Crystal growth

Polycrystalline $CeMgAl_{11}O_{19}$ samples were synthesized through a solid-state reaction, where CeO_2, MgO, and Al_2O_3 were mixed in precise stoichiometric ratios, ground, and pelletized for uniformity. The pellets were then calcined from 1250° to 1550°C for 72 hours, with intermediate grinding to improve purity and crystallinity. Single crystals were grown using the laser diode floating zone method, yielding high-quality $CeMgAl_{11}O_{19}$ crystals with well-defined *ab*-plane facets, suitable for magnetic and neutron scattering studies. X-ray photoelectron spectroscopy measurements show that all Ce ions are in the +3 valence (See fig. S5 for details).

Neutron and x-ray diffraction

Neutron diffraction data for $CeMgAl_{11}O_{19}$ were collected at room temperature using the TOPAZ instrument at the Spallation Neutron Source with neutron wavelengths of 0.4 to 3.5 Å. The measurements used time-of-flight methods, yielding wavelength-resolved Laue patterns. Absorption corrections were applied using the multiscan method. The crystal structure was determined to be in the hexagonal $P6_3/mmc$ space group, with lattice parameters $a = 5.5949(3)$Å and $c = 21.9286(19)$Å and a unit cell volume of $V = 594.46(7)$Å^3. The structure was refined using the JANA2020 software package, and the Ce deficiency in $CeMgAl_{11}O_{19}$ was found to be ~7%, similar to the Pr deficiency in $PrMg(Zn)Al_{11}O_{19}$ (*30*). See tables S1 and S2 for details.

Single-crystal x-ray diffraction data for $CeMgAl_{11}O_{19}$ were collected at room temperature using a Bruker Kappa D8 QUEST diffractometer with Mo Kα radiation. The structure was solved and refined using standard crystallographic software, revealing that $CeMgAl_{11}O_{19}$ crystallizes in the hexagonal $P6_3/mmc$ space group with lattice parameters $a = 5.5813(5)$Å and $c = 21.904(2)$Å. The structure consists of CeO_{12} polyhedra, Mg/AlO_4 tetrahedra, and AlO_6 octahedra, typical of magnetoplumbite-type structures. Ce^{3+} ions occupy specific Wyckoff positions, forming a distorted anticuboctahedral environment, while Mg^{2+} and Al^{3+} ions share positions, leading to partial occupancy and substitutional disorder that cannot be fully resolved by x-ray diffraction alone, necessitating neutron diffraction for differentiation. See tables S3 to S5 for details.

Magnetic susceptibility and heat capacity

dc magnetic susceptibilities were measured using a Quantum Design Magnetic Property Measurement System (MPMS). An oriented piece of $CeMgAl_{11}O_{19}$ crystal was mounted on an MPMS sample holder using GE varnish. ac susceptibility measurements were performed in a superconducting quantum interference device magnetometer on an MPMS with the iQuantum Helium-3 refrigerator option. A *c*-axis–oriented $CeMgAl_{11}O_{19}$ crystal was mounted on a straw sample holder using vacuum grease.

Heat capacity data were collected in a Quantum Design Physical Property Measurement System. An oriented piece of $CeMgAl_{11}O_{19}$ crystal was mounted on the heat capacity puck using Apiezon N Grease. The addenda heat capacity was previously measured and subtracted. Heat capacity data below 1.8 K were collected with a dilution refrigerator.

Neutron spectroscopy

Thermal inelastic neutron scattering measurements were performed on two polycrystalline samples of $CeMgAl_{11}O_{19}$ and $LaMgAl_{11}O_{19}$ (both 5.0 g in mass) using the MARI direct-geometry chopper spectrometer at the ISIS Neutron and Muon Source, UK. Data were collected at 5 K using incident neutron energies $E_i = 100$, 180, and 500 meV. The La-based nonmagnetic analog served as a phonon background reference. All measurements were performed in a closed-cycle refrigerator.

Low-energy inelastic neutron scattering measurements were conducted on a single crystal of $CeMgAl_{11}O_{19}$ using the cold-neutron disk-chopper spectrometer (AMATERAS) (*57*) at the Japan Proton Accelerator Research Complex (J-PARC). The crystal was aligned in the (*hk*0) scattering plane in a dilution refrigerator with a 4-T magnet along the *c* axis. We define the momentum transfer $\mathbf{Q}$ in 3D reciprocal space in Å^{-1} as $\mathbf{Q} = h\mathbf{a}^* + k\mathbf{b}^* + l\mathbf{c}^*$, where *h*, *k*, and *l* are Miller indices and $\mathbf{a}^* = \hat{a}2\pi/a$, $\mathbf{b}^* = \hat{b}2\pi/b$, and $\mathbf{c}^* = \hat{c}2\pi/c$ with $a = b = 5.5813(5)$Å and $c = 21.904(2)$ Å in the $P6_3/mmc$ space group. Incident neutron energies of $E_i = 1.5$ and 2.6 meV were used with instrumental energy resolution at elastic positions of 0.037 and 0.075 meV, respectively.

Supplementary Materials

This PDF file includes:

Supplementary Text
Figs. S1 to S7
Tables S1 to S5

REFERENCES

1. P. W. Anderson, Resonating valence bonds: A new kind of insulator? *Mater. Res. Bull.* **8**, 153–160 (1973).
2. A. Kitaev, Anyons in an exactly solved model and beyond. *Ann. Phys.* **321**, 2–111 (2006).
3. A. V. Chubukov, Fluctuations in spin nematics. *J. Phys. Condens. Matter* **2**, 1593–1608 (1990).
4. A. Läuchli, F. Mila, K. Penc, Quadrupolar phases of the $S = 1$ bilinear-biquadratic Heisenberg model on the triangular lattice. *Phys. Rev. Lett.* **97**, 087205 (2006).
5. S. Bhattacharjee, V. B. Shenoy, T. Senthil, Possible ferro-spin nematic order in $NiGa_2S_4$. *Phys. Rev. B* **74**, 092406 (2006).
6. K. Binder, A. P. Young, Spin glasses: Experimental facts, theoretical concepts, and open questions. *Rev. Mod. Phys.* **58**, 801–976 (1986).
7. J. A. Mydosh, *Spin Glasses: An Experimental Introduction* (CRC Press, 1993).
8. F. Mila, Quantum spin liquids. *Eur. J. Phys.* **21**, 499–510 (2000).
9. L. Balents, Spin liquids in frustrated magnets. *Nature* **464**, 199–208 (2010).
10. L. Savary, L. Balents, Quantum spin liquids: A review. *Rep. Prog. Phys.* **80**, 016502 (2017).
11. Y. Zhou, K. Kanoda, T.-K. Ng, Quantum spin liquid states. *Rev. Mod. Phys.* **89**, 025003 (2017).
12. C. Broholm, R. J. Cava, S. A. Kivelson, D. G. Nocera, M. R. Norman, T. Senthil, Quantum spin liquids. *Science* **367**, eaay0668 (2020).
13. A. Y. Kitaev, Fault-tolerant quantum computation by anyons. *Ann. Phys.* **303**, 2–30 (2003).
14. T.-H. Han, J. S. Helton, S. Chu, D. G. Nocera, J. A. Rodriguez-Rivera, C. Broholm, Y. S. Lee, Fractionalized excitations in the spin-liquid state of a kagome-lattice antiferromagnet. *Nature* **492**, 406–410 (2012).
15. F. Mingxuan, T. Imai, T.-H. Han, Y. S. Lee, Evidence for a gapped spin-liquid ground state in a kagome Heisenberg antiferromagnet. *Science* **350**, 655–658 (2015).
16. D. E. Freedman, T. H. Han, A. Prodi, P. Muller, Q.-Z. Huang, Y.-S. Chen, S. M. Webb, Y. S. Lee, T. M. McQueen, D. G. Nocera, Site specific X-ray anomalous dispersion of the geometrically frustrated kagomé magnet, herbertsmithite, $ZnCu_3(OH)_6Cl_2$. *J. Am. Chem. Soc.* **132**, 16185–16190 (2010).
17. Y. Shen, Y.-D. Li, H. Wo, Y. Li, S. Shen, B. Pan, Q. Wang, H. C. Walker, P. Steffens, M. Boehm, Y. Hao, D. L. Quintero-Castro, L. W. Harriger, M. D. Frontzek, L. Hao, S. Meng, Q. Zhang, G. Chen, J. Zhao, Evidence for a spinon fermi surface in a triangular-lattice quantum-spin-liquid candidate. *Nature* **540**, 559–562 (2016).
18. J. A. M. Paddison, M. Daum, Z. Dun, G. Ehlers, Y. Liu, M. B. Stone, H. Zhou, M. Mourigal, Continuous excitations of the triangular-lattice quantum spin liquid $YbMgGaO_4$. *Nat. Phys.* **13**, 117–122 (2017).
19. Z. Ma, J. Wang, Z.-Y. Dong, J. Zhang, S. Li, S.-H. Zheng, Y. Yunjie, W. Wang, L. Che, K. Ran, S. Bao, Z. Cai, P. Čermák, A. Schneidewind, S. Yano, J. S. Gardner, X. Lu, S.-L. Yu, J.-M. Liu, S. Li, J.-X. Li, J. Wen, Spin-glass ground state in a triangular-lattice compound $YbZnGaO_4$. *Phys. Rev. Lett.* **120**, 087201 (2018).
20. Z. Zhu, P. A. Maksimov, S. R. White, A. L. Chernyshev, Disorder-induced mimicry of a spin liquid in $YbMgGaO_4$. *Phys. Rev. Lett.* **119**, 157201 (2017).
21. I. Kimchi, A. Nahum, T. Senthil, Valence bonds in random quantum magnets: Theory and application to $YbMgGaO_4$. *Phys. Rev. X* **8**, 031028 (2018).
22. K. A. Ross, L. Savary, B. D. Gaulin, L. Balents, Quantum excitations in quantum spin ice. *Phys. Rev. X* **1**, 021002 (2011).
23. E. Lhotel, S. R. Giblin, M. R. Lees, G. Balakrishnan, L. J. Chang, Y. Yasui, First-order magnetic transition in $Yb_2Ti_2O_7$. *Phys. Rev. B* **89**, 224419 (2014).
24. A. Scheie, J. Kindervater, S. Zhang, H. J. Changlani, G. Sala, G. Ehlers, A. Heinemann, G. S. Tucker, S. M. Koohpayeh, C. Broholm, Multiphase magnetism in $Yb_2Ti_2O_7$. *Proc. Natl. Acad. Sci. U.S.A.* **117**, 27245–27254 (2020).
25. M. Ashtar, Y. X. Gao, C. L. Wang, Y. Qiu, W. Tong, Y. M. Zou, X. W. Zhang, M. A. Marwat, S. L. Yuan, Z. M. Tian, Synthesis, structure and magnetic properties of rare-earth $REMgAl_{11}O_{19}$ (RE = Pr, Nd) compounds with two-dimensional triangular lattice. *J. Alloys Compd.* **802**, 146–151 (2019).
26. H. Bu, M. Ashtar, T. Shiroka, H. C. Walker, Z. Fu, J. Zhao, J. S. Gardner, G. Chen, Z. Tian, H. Guo, Gapless triangular-lattice spin-liquid candidate $PrZnAl_{11}O_{19}$. *Phys. Rev. B* **106**, 134428 (2022).

27. C. P. Tu, Z. Ma, H. R. Wang, Y. H. Jiao, D. Z. Dai, S. Y. Li, Gapped quantum spin liquid in a triangular-lattice Ising-type antiferromagnet $PrMgAl_{11}O_{19}$. *Phys. Rev. Res.* **6**, 043147 (2024).
28. Z. Ma, S. Zheng, Y. Chen, R. Xu, Z.-Y. Dong, J. Wang, H. Du, J. P. Embs, S. Li, Y. Li, Y. Zhang, M. Liu, R. Zhong, J.-M. Liu, J. Wen, Possible gapless quantum spin liquid behavior in the triangular-lattice Ising antiferromagnet $PrMgAl_{11}O_{19}$. *Phys. Rev. B* **109**, 165143 (2024).
29. N. Li, A. Rutherford, Y. Y. Wang, H. Liang, Q. J. Li, Z. J. Zhang, H. Wang, W. Xie, H. D. Zhou, X. F. Sun, Ising-type quantum spin liquid state in $PrMgAl_{11}O_{19}$. *Phys. Rev. B* **110**, 134401 (2024).
30. Y. Cao, H. Bu, Z. Fu, J. Zhao, J. S. Gardner, Z. Ouyang, Z. Tian, Z. Li, H. Guo, Synthesis, disorder and Ising anisotropy in a new spin liquid candidate $PrMgAl_{11}O_{19}$. *Mater. Futures* **3**, 035201 (2024).
31. Y. Cao, A. Koda, M. D. Le, V. Pomjakushin, B. Liu, Z. Fu, Z. Li, J. Zhao, Z. Tian, H. Guo, U(1) Dirac quantum spin liquid candidate in triangular-lattice antiferromagnet $CeMgAl_{11}O_{19}$. *Sci. China Phys. Mech. Astron.* **68**, 267011 (2025).
32. Y. Li, G. Chen, W. Tong, L. Pi, J. Liu, Z. Yang, X. Wang, Q. Zhang, Rare-earth triangular lattice spin liquid: A single-crystal study of $YbMgGaO_4$. *Phys. Rev. Lett.* **115**, 167203 (2015).
33. P.-L. Dai, G. Zhang, Y. Xie, C. Duan, Y. Gao, Z. Zhu, E. Feng, Z. Tao, C. Huang, H. Cao, A. Podlesnyak, G. E. Granroth, M. S. Everett, J. C. Neuefeind, D. Voneshen, S. Wang, G. Tan, E. Morosan, X. Wang, H. Lin, L. Shu, G. Chen, Y. Guo, X. Lu, P. Dai, Spinon fermi surface spin liquid in a triangular lattice antiferromagnet $NaYbSe_2$. *Phys. Rev. X* **11**, 021044 (2021).
34. F. Ferrari, F. Becca, Dynamical structure factor of the $J_1 - J_2$ Heisenberg model on the triangular lattice: Magnons, spinons, and gauge fields. *Phys. Rev. X* **9**, 031026 (2019).
35. M. Drescher, L. Vanderstraeten, R. Moessner, F. Pollmann, Spectral functions of an extended antiferromagnetic $S = 1/2$ Heisenberg model on the triangular lattice. arXiv:2508.17292 (2025).
36. Y. Shen, Y.-D. Li, H. C. Walker, P. Steffens, M. Boehm, X. Zhang, S. Shen, H. Wo, G. Chen, J. Zhao, Fractionalized excitations in the partially magnetized spin liquid candidate $YbMgGaO_4$. *Nat. Commun.* **9**, 4138 (2018).
37. A. Banerjee, P. Lampen-Kelley, J. Knolle, C. Balz, A. A. Aczel, B. Winn, Y. Liu, D. Pajerowski, J. Yan, C. A. Bridges, A. T. Savici, B. C. Chakoumakos, M. D. Lumsden, D. A. Tennant, R. Moessner, D. G. Mandrus, S. E. Nagler, Excitations in the field-induced quantum spin liquid state of α-$RuCl_3$. *npj Quantum Mater.* **3**, 8 (2018).
38. S. Toth, B. Lake, Linear spin wave theory for single-q incommensurate magnetic structures. *J. Phys. Condens. Matter* **27**, 166002 (2015).
39. S. Miyashita, The ground state and thermodynamic properties of generalized Heisenberg models on the triangular lattice. *Prog. Theor. Phys. Suppl.* **87**, 112–126 (1986).
40. T. Momoi, M. Suzuki, Ground-state properties and phase diagram of the quantum *XXZ* antiferromagnet on a triangular lattice. *J. Phys. Soc. Jpn.* **61**, 3732–3744 (1992).
41. L. Seabra, T. Momoi, P. Sindzingre, N. Shannon, Phase diagram of the classical Heisenberg antiferromagnet on a triangular lattice in an applied magnetic field. *Phys. Rev. B* **84**, 214418 (2011).
42. O. A. Starykh, Unusual ordered phases of highly frustrated magnets: A review. *Rep. Prog. Phys.* **78**, 052502 (2015).
43. G. Marmorini, D. Yamamoto, I. Danshita, Umbrella-coplanar transition in the triangular *XXZ* model with arbitrary spin. *Phys. Rev. B* **93**, 224402 (2016).
44. D. Yamamoto, G. Marmorini, I. Danshita, Quantum phase diagram of the triangular-lattice *XXZ* model in a magnetic field. *Phys. Rev. Lett.* **112**, 127203 (2014).
45. D. Sellmann, X.-F. Zhang, S. Eggert, F. Lechermann, A. A. Tsirlin, Phase diagram of the antiferromagnetic *XXZ* model on the triangular lattice. *Phys. Rev. B* **91**, 081104 (2015).
46. D. Yamamoto, H. Ueda, I. Danshita, G. Marmorini, T. Momoi, T. Shimokawa, Exact diagonalization and cluster mean-field study of triangular-lattice *XXZ* antiferromagnets near saturation. *Phys. Rev. B* **96**, 014431 (2017).
47. H. J. Changlani, D. Kochkov, K. Kumar, B. K. Clark, E. Fradkin, Macroscopically degenerate exactly solvable point in the spin-1/2 kagome quantum antiferromagnet. *Phys. Rev. Lett.* **120**, 117202 (2018).
48. Z. Zhu, P. A. Maksimov, S. R. White, A. L. Chernyshev, Topography of spin liquids on a triangular lattice. *Phys. Rev. Lett.* **120**, 207203 (2018).
49. D. Dahlbom, H. Zhang, C. Miles, S. Quinn, A. Niraula, B. Thipe, M. Wilson, S. Matin, S. H. HetMankad, D. Pajerowski, S. Johnston, Z. Wang, H. Lane, Y. W. Li, X. Bai, M. Mourigal, C. D. Batista, K. Barros, Sunny.jl: A Julia package for spin dynamics. *J. Open Source Softw.* **10**, 8138 (2025).
50. K. W. Plumb, H. J. Changlani, A. Scheie, S. Zhang, J. W. Krizan, J. A. Rodriguez-Rivera, Y. Qiu, B. Winn, R. J. Cava, C. L. Broholm, Continuum of quantum fluctuations in a three-dimensional $S = 1$ Heisenberg magnet. *Nat. Phys.* **15**, 54–59 (2019).
51. S. Zhang, H. J. Changlani, K. W. Plumb, O. Tchernyshyov, R. Moessner, Dynamical structure factor of the three-dimensional quantum spin liquid candidate $NaCaNi_2F_7$. *Phys. Rev. Lett.* **122**, 167203 (2019).
52. X. Bai, J. A. M. Paddison, E. Kapit, S. M. Koohpayeh, J.-J. Wen, S. E. Dutton, A. T. Savici, A. I. Kolesnikov, G. E. Granroth, C. L. Broholm, J. T. Chalker, M. Mourigal, Magnetic excitations of the classical spin liquid $MgCr_2O_4$. *Phys. Rev. Lett.* **122**, 097201 (2019).
53. Z. Ma, Z.-Y. Dong, J. Wang, S. Zheng, K. Ran, S. Bao, Z. Cai, Y. Shangguan, W. Wang, M. Boehm, P. Steffens, L.-P. Regnault, X. Wang, Y. Su, S.-L. Yu, J.-M. Liu, J.-X. Li, J. Wen, Disorder-induced broadening of the spin waves in the triangular-lattice quantum spin liquid candidate $YbZnGaO_4$. *Phys. Rev. B* **104**, 224433 (2021).
54. C. L. Henley, Ordering due to disorder in a frustrated vector antiferromagnet. *Phys. Rev. Lett.* **62**, 2056–2059 (1989).
55. J. Villain, R. Bidaux, J.-P. Carton, R. Conte, Order as an effect of disorder. *J. Phys. France* **41**, 1263–1272 (1980).
56. A. Hickey, D. Lozano-Gómez, M. J. P. Gingras, Order-by-disorder without quantum zero-point fluctuations in the pyrochlore Heisenberg ferromagnet with Dzyaloshinskii-Moriya interactions. *Phys. Rev. B* **111**, 184434 (2025).
57. K. Nakajima, S. Ohira-Kawamura, T. Kikuchi, M. Nakamura, R. Kajimoto, Y. Inamura, N. Takahashi, K. Aizawa, K. Suzuya, K. Shibata, T. Nakatani, K. Soyama, R. Maruyama, H. Tanaka, W. Kambara, T. Iwahashi, Y. Itoh, T. Osakabe, S. Wakimoto, K. Kakurai, F. Maekawa, M. Harada, K. Oikawa, R. E. Lechner, F. Mezei, M. Arai, AMATERAS: A cold-neutron disk chopper spectrometer. *J. Phys. Soc. Jpn.* **80**, SB028 (2011).
58. C. Shan, S. Jin, T. Datta, D.-X. Yao, Torque equilibrium spin wave theory of Raman scattering in an anisotropic triangular lattice antiferromagnet with Dzyaloshinskii-Moriya interaction. *Phys. Rev. B* **103**, 024417 (2021).
59. S. El Hog, I. F. Sharafullin, H. T. Diep, H. Garbouj, M. Debbichi, M. Said, Frustrated antiferromagnetic triangular lattice with Dzyaloshinskii–Moriya interaction: Ground states, spin waves, skyrmion crystal, phase transition. *J. Magn. Magn. Mater.* **563**, 169920 (2022).
60. S. Pal, P. Sharma, H. J. Changlani, S. Pujari, Colorful points in the *XY* regime of *XXZ* quantum magnets. *Phys. Rev. B* **103**, 144414 (2021).

Acknowledgments: We thank C. Liu, H. Hu, J. Zhang, S. Zhang, Y. Gao, and S. Li for the discussions. **Funding:** The neutron scattering and ac magnetic susceptibility work at Rice were supported by the US DOE BES DE-SC0012311 (P.D.) and DE-SC0026179 (P.D. and E.M.). The single crystal growth work was supported by the Robert A. Welch Foundation under grant no. C-1839 (P.D.). Crystal growth at Rutgers University was supported by the DOE under Grant No. DOE: DE-FG02-07ER46382. The theoretical work done by C.L. and L.B. was supported by the DOE, Office of Science, BES under award no. DE-FG02-08ER46524 and the Simons Collaboration on Ultra-Quantum Matter. C.L. acknowledges the fellowship support from the Gordon and Betty Moore Foundation through the Emergent Phenomena in Quantum Systems (EPiQS) program. Z.M. acknowledges the National Natural Science Foundation of China with grant no. 12204160. C.W. acknowledges the National Research Foundation of Korea (NRF), Ministry of Science and ICT (no. 2022M3H4A1A04074153). G.T.M. and J.Y.C. acknowledge the Welch Foundation, AA-2056-20240404. The neutron scattering experiment at the MLF of J-PARC was performed under proposal no. 2022B0242. The neutron diffraction experiment was performed at the Spallation Neutron Source, a DOE Office of Science User Facility operated by Oak Ridge National Laboratory. The beam time was allocated to TOPAZ on proposal number IPTS-31845. **Author contributions:** Conceptualization: B.G., T.C., C.L., Z.M., J.Y.C., J.T.R., L.B., and P.D. Methodology: B.G., T.C., C.L., N.M., S.O.-K., X.X., G.T.M., E.M., J.Y.C., J.T.R., L.B., X.H., and P.D. Investigation: B.G., T.C., C.L., M.L.K., N.M., S.O.-K., X.X., C.W., G.T.M., K.R., S.J.M., J.T.R., X.H., X.W., M.D.L., E.M., J.Y.C., L.B., and P.D. Resources: B.G., T.C., C.L., N.M., S.O.-K., X.H., X.W., M.D.L., E.M., J.Y.C., S.-W.C., G.T.M., J.T.R., L.B., and P.D. Data curation: T.C., N.M., S.O.-K., X.H., M.D.L., J.Y.C., G.T.M., J.T.R., and P.D. Validation: B.G., T.C., C.L., X.H., X.W., M.D.L., E.M., J.Y.C., S.-W.C., G.T.M., J.T.R., L.B., Z.M., and P.D. Formal analysis: B.G., T.C., C.L., K.R., X.W., M.D.L., J.Y.C., G.T.M., J.T.R., and L.B. Visualization: B.G., T.C., C.L., K.R., G.T.M., E.M., J.Y.C., J.T.R., and Z.M. Supervision: E.M., S.-W.C., J.Y.C., T.C., L.B., Z.M., J.T.R., and P.D. Funding acquisition: E.M., S.-W.C., J.Y.C., L.B., Z.M., and P.D. Project administration: T.C., J.Y.C., L.B., Z.M., and P.D. Software: T.C. Writing—original draft: B.G., T.C., C.L., S.Z., O.T., Z.M., L.B., and P.D. Writing—review and editing: B.G., T.C., C.L., M.L.K., S.Z., Z.M., C.W., G.T.M., K.R., S.J.M., J.T.R., X.H., X.W., M.D.L., E.M., J.Y.C., S.-W.C., O.T., L.B., and P.D. **Competing interests:** The authors declare that they have no competing interests. Certain equipment, instruments, software, or materials are identified in this paper to specify the experimental procedure adequately. This identification is not intended to imply recommendation or endorsement of any product or service by NIST, nor is it intended to imply that the materials or equipment identified are necessarily the best available for the purpose. **Data, code, and materials availability:** All data and code needed to evaluate and reproduce the results in the paper are present in the paper and/or the Supplementary Materials. No custom code was used beyond standard data-reduction and analysis software. Materials are available from the corresponding authors upon reasonable request.

Submitted 9 November 2025
Accepted 29 January 2026
Published 6 March 2026
10.1126/sciadv.aed7778

ScienceAdvances

Spin excitation continuum from degenerate states in the mixed ferro-antiferromagnetic exchange system $CeMgAl_{11}O_{19}$

Bin Gao, Tong Chen, Chunxiao Liu, Mason L. Klemm, Shu Zhang, Zhen Ma, Xianghan Xu, Choongjae Won, Gregory T. McCandless, Karthik Rao, Naoki Murai, Seiko Ohira-Kawamura, Stephen J. Moxim, Jason T. Ryan, Xiaozhou Huang, Xiaoping Wang, Manh Duc Le, Emilia Morosan, Julia Y. Chan, Sang-Wook Cheong, Oleg Tchernyshyov, Leon Balents, and Pengcheng Dai

Sci. Adv. **12** (10), eaed7778. DOI: 10.1126/sciadv.aed7778

Science Advances (ISSN 2375-2548) is published by the American Association for the Advancement of Science. 1200 New York Avenue NW, Washington, DC 20005. The title *Science Advances* is a registered trademark of AAAS.